

## Thermal Management Using a Hypervapotron; Part II: Additional Controlling Parameter

**Ronald D. Boyd**

Prairie View A&M University, Prairie View, TX 77446-0519  
rdboyd@pvamu.edu

### Abstract

The hypervapotron (HV) has been demonstrated to be a superior thermal management (TM) and high heat flux removal (HHFR) technique for fusion reactor plasma-facing component applications involving a single-side absorbed heat flux (up to between 20 and 30 MW/m<sup>2</sup>). However, the conjugate heat transfer HV flow channel (HVFC) performance only can be optimized completely when the related HHFR controlling parameters have been identified. In an earlier work, Part I of the present effort identified four HV controlling TM and HHFR dimensionless parameters. In the present work, four additional dimensionless primary controlling parameters and five secondary controlling parameters have been identified. The controlling parameters include effects of: (1) most geometric specifications of the array of fins; (2) variations in the HV wall thermal conductivity and heat transfer coefficient; (3) effective Biot numbers characterizing two-dimensional effects which include the fin array, a typical fin, and the vertical side wall; (4) HVFC unobstructive portion flow aspect ratio, and (5) the HVFC wall aspect ratio. Future work should assess the sensitivity of these parameters.

### 1. Introduction

As advancements are made in alternative energy options, thermal management (TM) and high heat flux removal (HHFR) will become increasingly important. For example, the International Thermonuclear Experimental Reactor (ITER) is being constructed (see Figure 1) in France and will be the world's largest tokamak fusion reactor [1]. "...The 'tokamak' concept involves...magnetic confinement..." of a 150 million °C plasma which is produced from a fusion reaction of a mixture of deuterium and tritium--two isotopes of hydrogen [1]. "Strong magnetic fields are used to keep the plasma away from the walls..." However, there are regions in the reactor where the incident absorbed steady-state heat flux ( $\dot{q}_{\infty}$ ) can be and sometimes exceed the range between 5.0 and 15 MW/m<sup>2</sup> [2, 3].

One device which will experience heat fluxes near this upper limit is the divertor (see Figure 2). "Situated along the bottom of the [reactor vacuum] vessel, ...the divertor is one of the key components of ITER. ...Its function is [HHFR] and [removal of] helium ash... & other impurities"--all of which are "...products of the fusion reaction" [1]. Each remotely-removable cassette (see Figure 2b) of the divertor has three plasma-facing components (PFCs) or targets: (1) the inner and outer vertical targets, and (2) the dome [1].

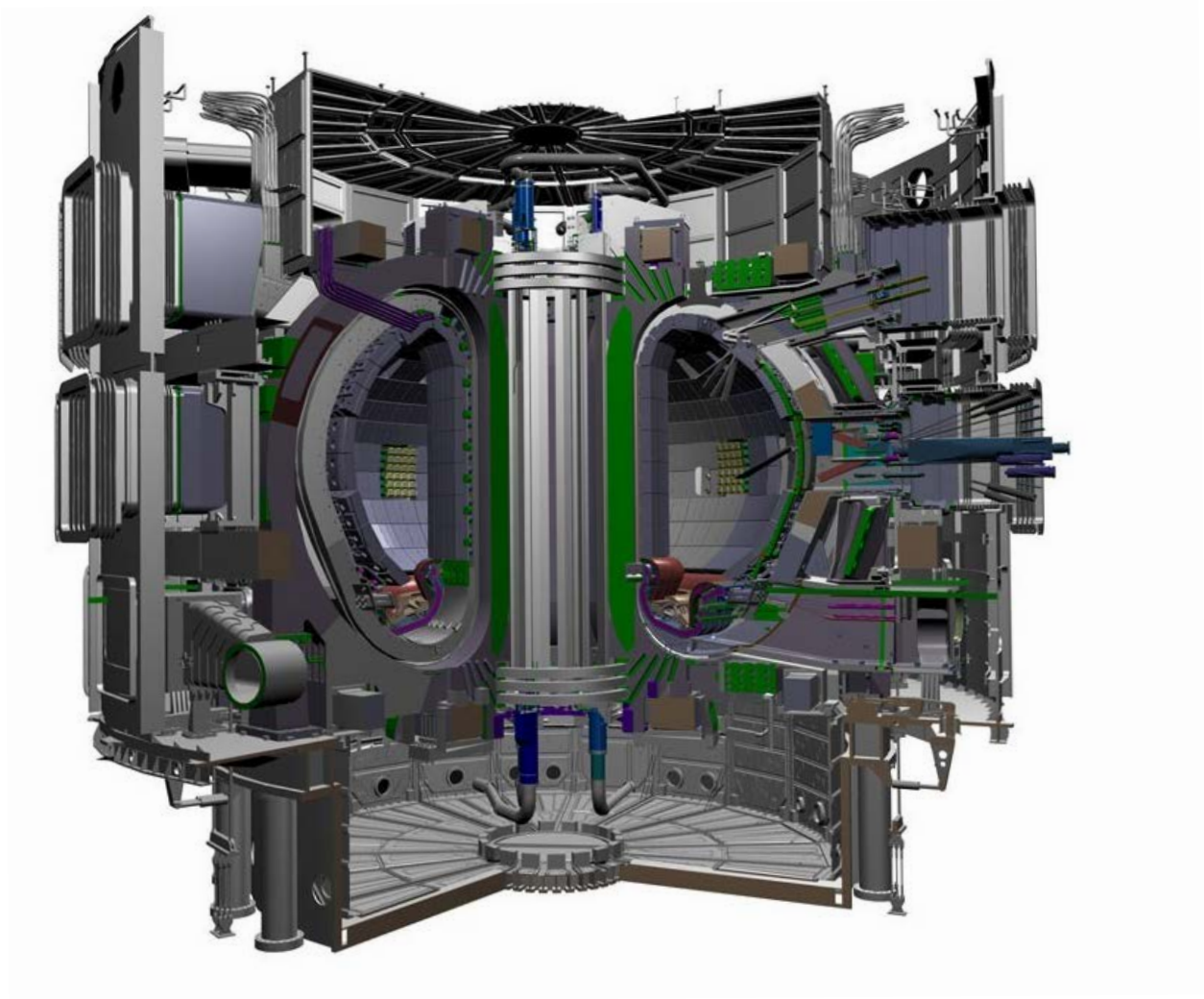
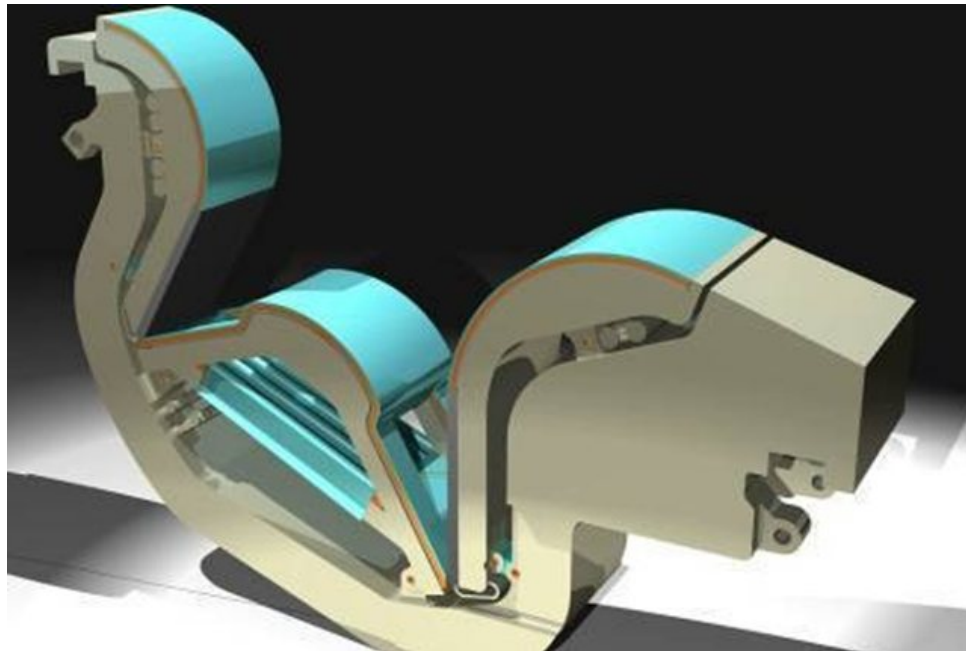


Figure 1 The ITER Fusion Reactor [1].



(2a)



(2b)

Figure 2 “The divertor (see Figure 2a) is one of the key components in the ITER Machine” [1]. A cross-section of it is shown in Figure 2b where three plasma-facing components or targets can be seen. These targets are the: (1) inner and outer vertical targets and, (2) dome [1].

“These targets are situated at the intersection of magnetic field lines where the high-energy plasma particles strike [them. The particles’] kinetic energy is transformed into heat...; [and hence,] the heat flux received by these [PFCs] is extremely intense and requires active water cooling.” In the case of water cooling, strict TM design criteria must be established so that the critical heat flux (CHF) is not exceeded. The CHF is the maximum heat flux at the water-solid coolant channel interface, beyond which the heated area could be irreversibly damaged, compromised, or even destroyed [4, 5].

The blanket modular wall is another example of where HHFR and TM is required. This wall covers the interior surfaces of the vacuum vessel; and, its detachable first wall can experience heat fluxes between 0.5 and 5.0 MW/m<sup>2</sup> [3].

Among the many alternative TM and HHFR schemes and devices investigated to accommodate the above high heat flux demands, the hypervapotron (see Figure 3) has been used over the past thirty (30) years to demonstrate HHFR capability up to heat fluxes between 20.0 and 30.0 MW/m<sup>2</sup> [6] with lower pumping power than some other alternatives [2]. Clearly, the hypervapotron (HV) should be a prime TM and HHFR device for ITER and many other future demanding HHFR applications. In the past, design improvements to the HV have “been traditionally sought experimentally which is both inefficient and costly” [6]--especially when improvements are sought without knowledge of the TM and HHFR controlling parameters.

Therefore, a HV is an excellent candidate for TM in cases where single-side HHFR is of prime importance. In order to effectively characterize additional optimal operating characteristics using computational fluid dynamics (CFD) and/or experimental approaches (EA, and/or design approaches (DA)), knowledge of the controlling TM hypervapotron parameters would be essential for timely HHFR enhancement configuration identification. The HHFR in a HV involves conjugate heat transfer which is characterized by both flow parameters (e.g., the Reynolds and Prandtl numbers) as well flow channel parameters (e.g., the Biot number). Further, there will be also unique geometric and heat transfer parameters associated with the hypervapotron fins. A combination of all these parameters must establish a basis for defining optimal [3, 8] operating conditions. From the HV model (see Figure 4) used in Part I of this work [9], four controlling parameters (see Figure 2) were identified: 1)

$$Bi = h_{eq} t / k_1, \quad (2) \quad w_c / t, \quad (3) \quad (w/2 - w_c) / L^*, \quad \text{and} \quad (4) \quad q_{\infty}^* w_c / k T^*.$$

Although most of these quantities are illustrated in Figures 4 and 5, Bi is the Biot number which includes the HV wall heat transfer and geometric parameters, L\* is a yet unidentified characteristic length, and T\* is a characteristic HV temperature (in degrees Celsius).

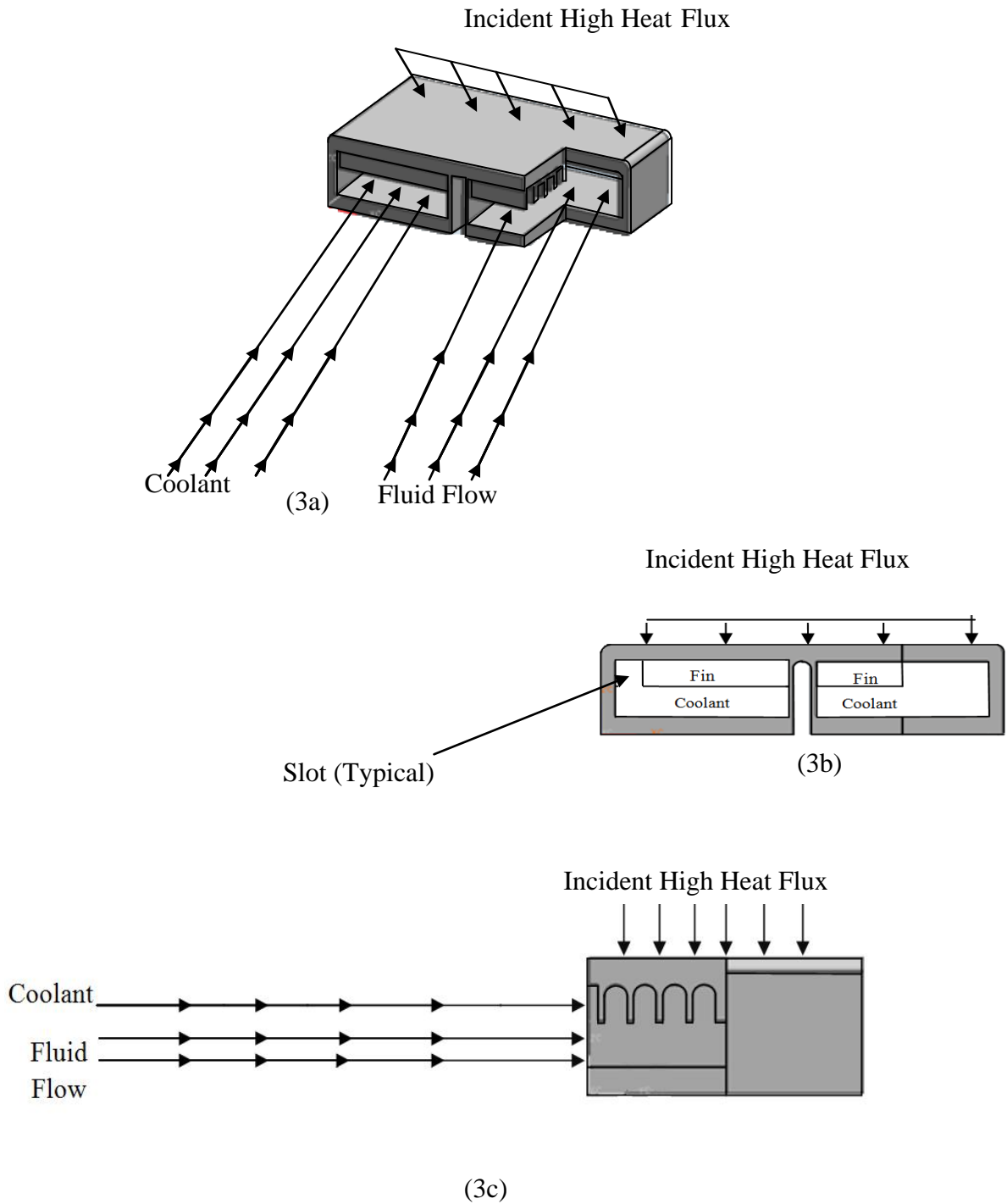


Figure 3 Another possibility for TM is a hypervapotron which is here subjected to a single-side incident (absorbed) heat flux with an internally flowing coolant [7].

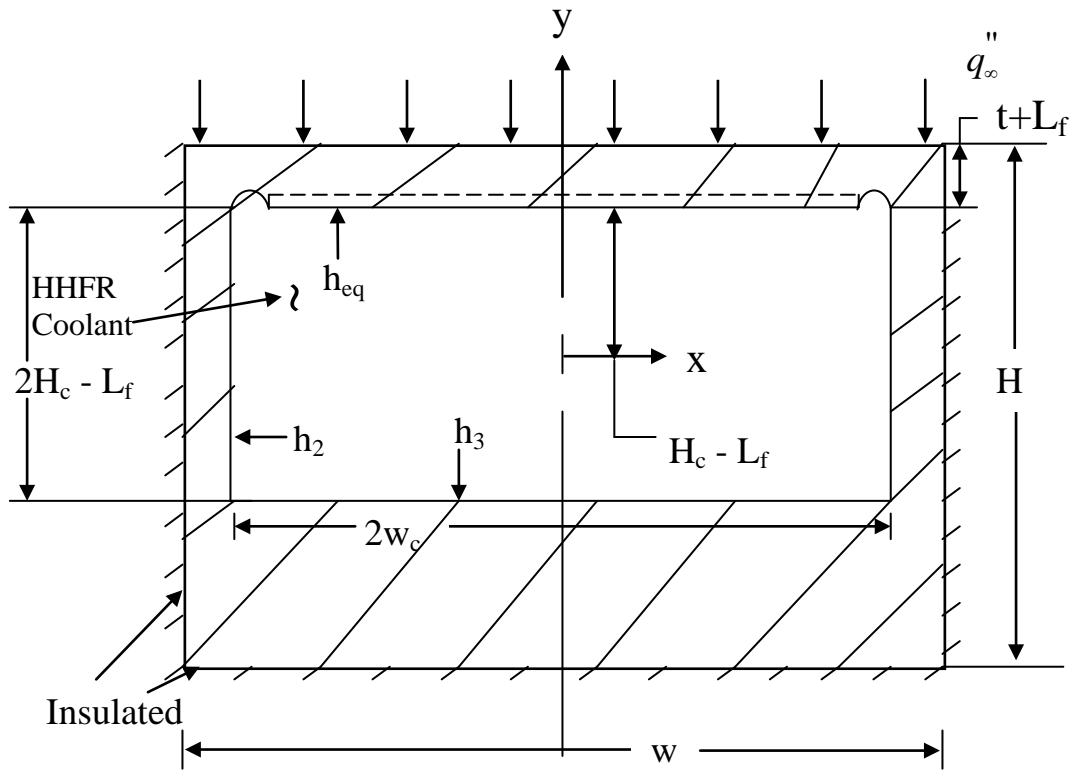


Figure 4 Simplified 2-D HFC Unit Cell Used for Modeling.

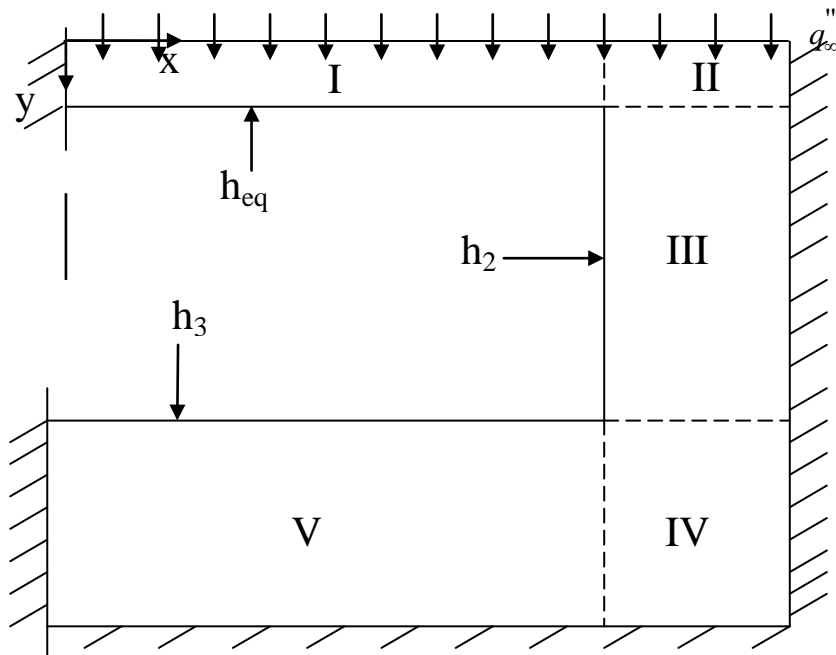


Figure 5 2-D HFC Unit Cell Model Domains With the Origin for the y-axis Changed So That Simpler Conditions Result.

Once HHFR HV controlling parameters have been identified, a suitable [10] computational fluid dynamic (CFD) code must be used for HV design and optimization. Milnes, Burns, and Drikakis [6] recommended a RANS-based multiphase CFD code. Pascal-Ribot et al. [11] recommended the coupled computer codes Neptune CFD and Syrthes. Ovchinniko, et al. [12] investigated a HHFR enhancing modification to the HV which included for example “chevron” fins or fins which are at a different angle relative to the coolant flow as compared to the HV fin-coolant normal flow angle. Lee et al. [13] use the ANSYS CFX-II CFD code for HV simulation comparisons with experimental data and obtained large differences. For a 2<sup>nd</sup> qualification of the ITER first wall, Lee et al [14] had better agreement. Wang, Song, and Huang [2, 15] studied six (6) HV fin configurations and concluded that the triangle fin “against the flow direction” was most effective. Mazul et al. [16] upgraded the ITER first wall design to improve resistance to electromagnetic loads while using a HV coolant channel with CuCrZr – SS bimetallic walls. Cattadori et al. [17] presented boiling curves and other data for a modified HV for high heat fluxes (above 10 MW/m<sup>2</sup>) and as a function of the fin geometric dimensions. Escourbiac et al. [18], based on HV tests up to 25 MW/m<sup>2</sup> with up to 1000 cycles and up to 15 MW/m<sup>2</sup> with up to 3000 cycles (and a critical heat flux higher than 30 MW/m<sup>2</sup>), concluded that CuCrZr HV armoured with flat tiles of carbon fibre composite Sepcarb NS31 is a mature industrial solution for ITER.

The focus of this work is to investigate some fundamental aspects of high heat flux removal (HHFR) that will increase the possibility of determining additional HHFR controlling parameters for a HV which is subjected to a heat flux from a single-side.

## 2. Model

Although the incident heat flux ( $q''_{\infty}$ ) is a significant function of the flow channel axial coordinate, it will be assumed constant for the initial modeling effort. This limitation will be relaxed and included in future work. The hypervapotron flow channel (HFC) shown in Figure 4 is a unit cell of an array of such units which make up the basic aspects of the PFC HHFR system. This figure will be used to develop the model for the 2-D HFC unit cell. The model was subdivided into the domains shown in Figure 5. The two-dimensional steady-state thermal diffusion equation was used to obtain the local wall temperature distributions for Domains I [9], II, and III.

## 3. Model Development Domain Results

The results for Domain I (with  $k$  now being replaced by  $k_1$ ) was completed by Boyd [9] in Part I of this work. As Boyd noted, complexities can be avoided if the  $y$ -coordinate is relocated to the location shown in Figure 5. The remaining analysis employs this coordinate relocation. An illustration of how all domains were examined is given below for Domain II and in references [9] for Domain I.

Because of the three nonhomogeneities in the  $\theta_{II}$  formulation, let

$$\theta_{II}(x, y) = \theta_{II_1}(x, y) + \theta_{II_2}(x, y) + \theta_{II_3}(x, y); \quad (1)$$

where the boundary conditions are summarized in Figure 6.

Therefore,

$$\theta_{II_1}(x, y) = \sum_{n=1}^{\infty} E_{II_n} \left[ e^{\lambda_{II_n} x} + e^{\lambda_{II_n} (w-x)} \right] \cos(\lambda_{II_n} y), \quad (2a)$$

where,

$$\lambda_{II_n} = \frac{n\pi}{2t}, \text{ with } n = 1, 3, 5, \dots; \quad (2b)$$

and the coefficient  $E_{II_n}$  is given by

$$E_{II_n} = \frac{\int_0^t \theta_I(x, y) \Big|_{x=w_c} \cos(\lambda_{II_n} y) dy}{\left[ e^{\lambda_{II_n} w_c} + e^{\lambda_{II_n} (w-w_c)} \right] \int_0^t \cos^2(\lambda_{II_n} y) dy}, \quad (2c)$$

where  $\theta_I(x, y)$  is given by Boyd [9]. Another coordinate transformation (see Figure 6) was used to obtain a simplified form for  $\theta_{II_2}$ ; so that,

$$\theta_{II_2} = \sum_{n=1}^{\infty} E_{II_{2n}} \cos(\lambda_{II_{2n}} x_1) \left[ e^{\lambda_{II_{2n}} y} - e^{\lambda_{II_{2n}} (2t-y)} \right] \quad (3a)$$

where,

$$E_{II_{2n}} = \frac{\int_0^{\frac{w}{2}-w_c} \left[ \frac{-q_{oo}}{\lambda_{II_{2n}} k_{II} \left( 1 + e^{2t \lambda_{II_{2n}}} \right)} \right] \cos(\lambda_{II_{2n}} x_1) dx_1}{\int_0^{\frac{w}{2}-w_c} \cos^2(\lambda_{II_{2n}} x_1) dx_1}. \quad (3b)$$

$$n = 1, 3, 5, \text{ and} \quad (3c)$$

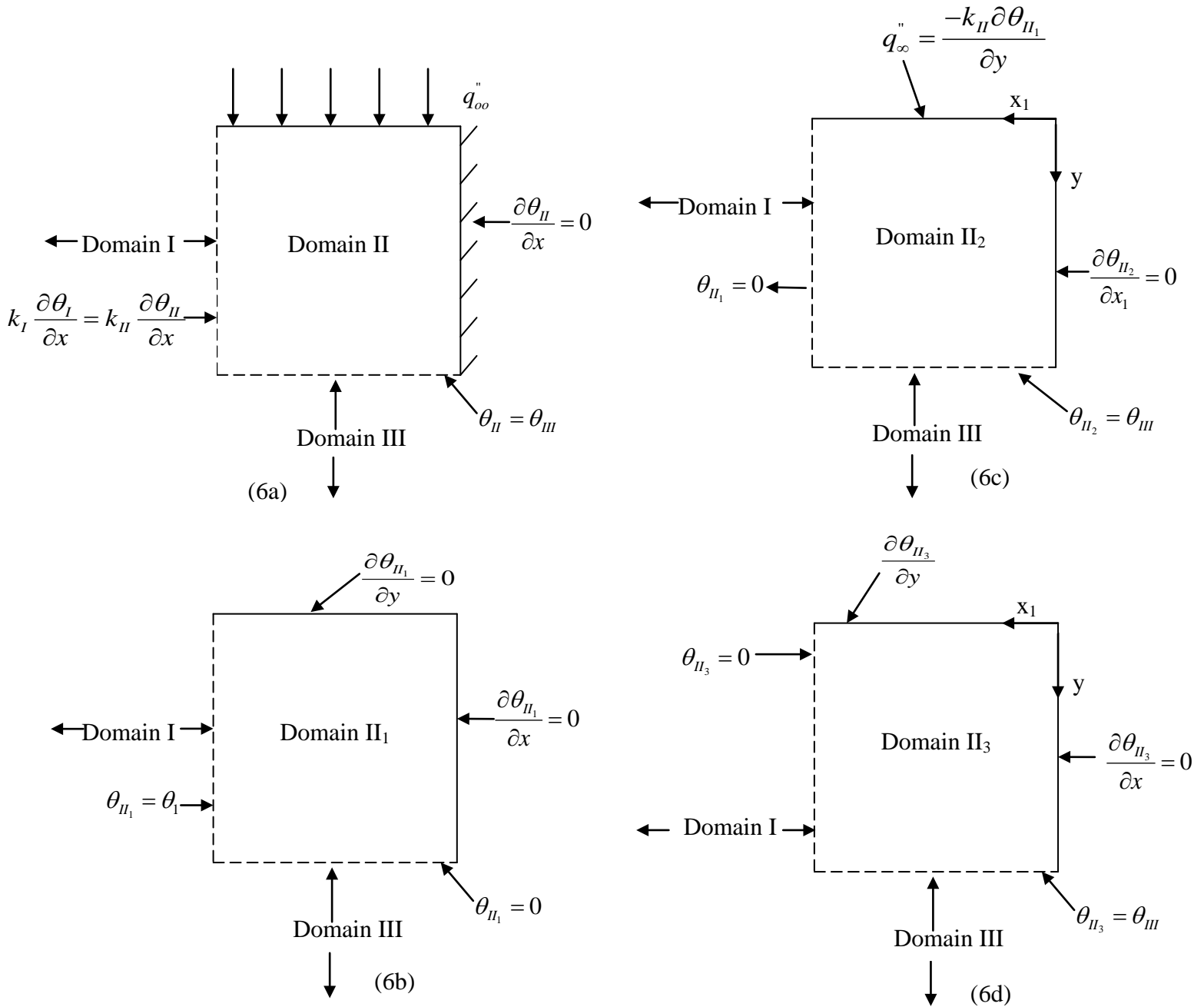


Figure 6 Domain II (6a), and its Sub-Domains II<sub>1</sub>, II<sub>2</sub>, and II<sub>3</sub> (Figs. 6b, 6c, 6d, respectively).

$$\lambda_{II_{2n}} = \frac{n}{\left(\frac{w}{2} - w_c\right)} \frac{\pi}{2} = \frac{n\pi}{(w - 2w_c)} \dots, \quad (3d)$$

The final sub-domain temperature distribution for Domain II is given by

$$\theta_{II_3} = \sum_{n=1}^{\infty} E_{II_{3n}} \cos(\lambda_{II_{2n}} x_1) \left[ e^{\lambda_{II_{3n}} t} + e^{-\lambda_{II_{3n}} y} \right], \quad n = 1, 3, 5, 7, \dots, \lambda_{II_{3n}} = \frac{n\pi}{(w - 2w_c)}, \text{ and} \quad (4a)$$

$$E_{II_{3n}} = \frac{\int_0^{\frac{w}{2} - w_c} \left[ \frac{\theta_{II} |_{y=t}}{\left( e^{\lambda_{II_{3n}} t} + e^{-\lambda_{II_{3n}} t} \right)} \right] \cos(\lambda_{II_{3n}} x_1) dx_1}{\int_0^{\frac{w}{2} - w_c} \cos^2(\lambda_{II_{3n}} x_1) dx_1} \quad (4b)$$

For Domain III, let

$$\theta_{III}(x, y) = \theta_{III_1} + \theta_{III_2}, \quad (5)$$

where

$$\theta_{III_1} = \sum_n D_{III_n} \cos(\lambda_{III_n} x_1) \left[ e^{\lambda_{III_n} y} - e^{\lambda_{III_n} (2[t+H_c] - y)} \right], \quad (6a)$$

$$D_{III_n} = \frac{\int_0^{\frac{w}{2} - w_c} \left[ \frac{\theta_{II} |_{y=t}}{\left( e^{\lambda_{III_n} t} - e^{\lambda_{III_n} (2H_c + t)} \right)} \right] \cos(\lambda_{III_n} x_1) dx_1}{\int_0^{\frac{w}{2} - w_c} \cos(\lambda_{III_n} x_1) dx_1}, \quad (6b)$$

$$\frac{1}{Bi_2} = \frac{\cot \left[ \lambda_{III_n} \left( \frac{w}{2} - w_c \right) \right]}{\left[ \lambda_{III_n} \left( \frac{w}{2} - w_c \right) \right]}, \text{ and} \quad (6c)$$

$$Bi_2 = \frac{h_2 \left( \frac{w}{2} - w_c \right)}{k_{III}}, \quad (6d)$$

where  $n$  and  $\lambda_{III_1}$  will be determined by eq (6c). Because of the similarity between the convective-conductive boundary condition of Domains III<sub>1</sub> and III<sub>2</sub>,  $\lambda_{III_2} = \lambda_{III_1}$ . Further,

$$\theta_{III_2} = \sum_n D_{III_{2n}} \cos(\lambda_{III_{2n}} x_1) \left[ e^{\lambda_{III_n} y} - e^{\lambda_{III_n} (2t-y)} \right], \quad (7a)$$

where

$$D_{III_{2n}} = \frac{\int_0^{\frac{w}{2}-w_c} \left[ \frac{\theta_{IV} \Big|_{y=t+2H_c}}{\left( e^{\lambda_{III_n} (t+2H_c)} - e^{\lambda_{III_n} (t-2H_c)} \right)} \right] \cos(\lambda_{III_n} x_1) dx_1}{\int_0^{\frac{w}{2}-w_c} \cos^2(\lambda_{III_n} x_1) dx_1}. \quad (7b)$$

The last effect that will be included in this Part is the hypervapotron fins. In this model, the effect of the fins is completely included in  $h_{eq}$ , which is given by [19]

$$h_{eq} = h_1 \eta_o \left( \frac{A_T}{A_b} \right) \quad (8)$$

where a 1-D fin analysis was used and  $h_1$  is the mean heat transfer coefficient for the hypervapotron fin sides ( $h_e$  will later be used as the fin tip heat transfer coefficient) and bare areas between the fins,  $\eta_o$  is the overall fin surface effectiveness,  $A_T/A_b$  is the ratio of the total surface area of the finned surface to that of the downward facing flow channel surface if it did not have fins. In addition, the classical literature (e.g. [19]) defines  $\eta_o$  as

$$\eta_o = 1 - \frac{NA_f}{A_T} (1 - \eta_f) \quad (9)$$

where a 1-D fin analysis is assumed,  $N$  is the number of fins used in a monoblock unit cell,  $A_f$  is the exposed surface area of a single fin, and  $\eta_f$  is the fin efficiency. For the straight, rectangular cross-section fins of the typical hypervapotron,  $\eta_f$  is given by

$$\eta_f = \frac{1}{\left( Bi_{f_1} / \delta^* \right)^{\frac{1}{2}} (1 + \delta^*)} \left[ \frac{\sinh(mL_f) + Bi_{f_2} \cosh(mL_f)}{\cosh(mL_f) + Bi_{f_2} \sinh(mL_f)} \right] \quad (10)$$

and where  $\delta$  is the fin thickness,  $L_f$  is the fin length,

$$w_1 = 2w_c - 2w_f, \delta^* = \left[ \frac{\delta/L_F}{2 \left( 1 + \frac{\delta}{w_1} \right)} \right], Bi_{f_1} = \frac{h_1 L_f}{k_I}, Bi_{f_2} = \frac{h_1}{mk_I}, \text{ and } m = \left[ 2h_1 (\delta/w_1 + 1)/k_I \delta \right]^{\frac{1}{2}}. \quad (11)$$

Further, other contributions to the above are the following area ratios,

$$\frac{A_T}{A_b} = \frac{2 \frac{L_f}{\delta} \left( 1 + \frac{\delta}{w_1} \right) + 1}{\left( \frac{S}{\delta} \right) - 1} = \frac{\delta^{*^{-1}} + 1}{\frac{S}{\delta} - 1}, \text{ and } \frac{NA_f}{A_T} = \left[ 1 + \frac{\left( \frac{S}{\delta} - 1 \right)}{\left( \delta^{*^{-1}} + 1 \right)} \right]^{-1}. \quad (12)$$

#### 4. Additional HV Controlling Parameters

The characteristic reference temperature ( $T^*$ ) was included in Part I [9] but was not specified. From Domain II,  $T^*$  could be defined using eqs (3b) and (3d) as

$$\frac{q_{\infty}'' \left( \frac{w}{2} - w_c \right)}{k_{II}} \quad (13)$$

or using Domain I, it could be defined as

$$T^* = \frac{q_{\infty}'' w_c}{k_I}. \quad (14)$$

Since eq (15) will result in the highest reference temperature, this will be used for  $T^*$ , with  $T^*$  being in units of degrees Celsius. Further, the unspecified characteristic length ( $L^*$ ) in Part I can now be determined by referring to eqs (4c) and (4d), and it is given by

$$L^* = t. \quad (15)$$

When  $T^*$  is used in eq. (3), the following additional parameter results:

$$\frac{\left( \frac{w}{2} - w_c \right) k_I}{w_c k_{II}} \text{ or } \frac{k_I}{k_{II}} \left( \frac{w}{2w_c} - 1 \right). \quad (16)$$

From eqs (6a), (6b), and (7b) three additional parameters appear:

$$Bi_2 = \frac{h_2 \left( \frac{w}{2} - w_c \right)}{k_{III}}, \quad \frac{2H_c + t}{\frac{w}{2} - w_c}, \quad \text{and} \quad \frac{2H_c - t}{\frac{w}{2} - w_c}, \quad (17)$$

where the latter two parameters appear to be similar. For the fins, the parameters are  $\eta_o$ , and  $\frac{A_T}{A_b}$  where m is given in eq (11). It should be noted that  $\eta_o$ ,  $\eta_f$ ,  $\frac{A_T}{A_b}$ ,  $\frac{NA_f}{A_T}$  are controlled by the following parameters: (1)  $mL_f$ , (2)  $\delta^*$ , (3)  $S/\delta$ , (4)  $Bi_{f_1}$ , and (5)  $Bi_{f_2}$ .

The conjugate heat transfer parameters can be defined as internal and external. Internal or fluid flow parameters such as the Reynolds and Prandtl numbers will have a direct influence on the heat transfer coefficients which appeared in specified boundary conditions. The effect of these internal parameters is included in resulting HV parameters summarized below. Another internal parameter which will greatly influence the convective HHFR capability is  $(H_c - L_f/2)/w_c$ , which represents the unobstructed flow aspect ratio (AR). The AR will clearly affect [20, 21] HHFR enhancement.

## 5. Conclusion

In addition to the three controlling parameters identified in Part I, four additional primary hypervapotron controlling parameters have been identified in the present work:

$$(1) \frac{k_I}{k_{II}} \left( \frac{w}{2w_c} - 1 \right), \quad (2) Bi_2 = \frac{h_2 \left( \frac{w}{2} - w_c \right)}{k_{III}}, \quad (3) \frac{2H_c + t}{\frac{w}{2} - w_c}, \quad \text{and} \quad (4) (H_c - L_f/2)/w_c. \quad (18)$$

In addition, the reference temperature (in degrees Celsius) and length are  $T^* = q_\infty'' w_c / k_I$  and  $L^* = t$ , respectively. Further, the hypervapotron HHFR is also related to  $\eta_o$ ,  $\eta_f$ ,  $\frac{A_T}{A_b}$ ,  $\frac{NA_f}{A_T}$  along with the fin effectiveness [19] which are functions of the following secondary parameters: (1)  $mL_f$ , (2)  $\delta^*$ , (3)  $Bi_{f_2}$ , (4)  $S/\delta$ , and (5)  $Bi_{f_1}$ .

The above primary and secondary controlling parameters along with those identified in Part I [9] are directly related to the high heat flux removal in a hypervapotron; and they may be useful for optimizing operating configurations and conditions. More parameters will result from analyses of Domains IV and V, which will be included in Part III (Summary of HV Parameters) of this

work. Finally, future work should also address the sensitivity of the above controlling parameters.

## 6. Nomenclature

$A_b$	total surface area of the top inner flow channel surface without the fins being added to that surface
$A_T$	total surface area of the top inner flow channel surface including the fins
$AR$	$(H_c - L_f/2)/w_c$
$Bi$	$h_{eq} t/k$
$h_{eq}$	equivalent heat transfer coefficient (HTC) for the upper hypervapotron (HV) inner flow channel surface (see eq. (8))
$h_1$	mean HTC of the HV finned side surfaces and bare surface between fins
$h_2$	mean HTC on the flow channel (FC) inner vertical surfaces
$h_3$	mean HTC on the FC bottom surface
$H$	outside height of HV (see Fig. 4)
$H_c$	one-half of the height from the base (or root) of the fin to the bottom inside surface of the HV flow channel (see Fig. 4)
$k$	mean flow channel wall thermal conductivity
$L_f$	length of the HV rectangular straight fin
$L^*$	reference length
$q''$	local heat flux
$q_{\infty}$	single-side, incident, absorbed heat flux
$S$	fin pitch
$t$	HV upper wall thickness from the surface with the single-side incident (absorbed) heat flux to the root or base of the fins (see Fig.4)
$T$	local flow channel wall temperature
$T_b$	bulk temperature of coolant
$T^*$	reference temperature in degrees Celsius
$W$	outside width of the HV (see Fig. 4)
$w_c$	HV inside flow channel half width (see Fig. 5)
$w_f$	width of the HV slot on either side of the fins (see Fig. 4)
$x$	x-coordinate (see Figs. 4 through 6)
$y$	y-coordinate (see Figs. 4 through 6)

### *Greek symbols*

$\eta_o$	overall fin surface effectiveness
$\theta$	temperature and/or temperature difference (relative to $T_b$ ) used in each of the domains
$\lambda$	eigenvalue
$\delta$	fin thickness

### *Subscripts*

f	refers to a specific fin characteristic
n	integer index for the eigenvalues
I	index used for Domain I
II	index used for Domain II
III	index used for Domain III
IV	index used for Domain IV
V	index used for Domain V

## 7. Acknowledgments

This work was supported by the US Department of Energy under contract number DE-FG02-97ER54452. The author is appreciative to Vivian J. Glover-Simmons and the Thermal Science Research Center personnel for their steadfast and positive support.

## 8. References

- [1.] [www.iter.org/mach](http://www.iter.org/mach)
- [2.] Z. Wang, Y. Song, and S. Huang, Design of the hypervapotron module for the EAST device, *Fusion Engineering and Design*, Vol. 87, 2012, pp. 868-871.
- [3.] D. L. Youchison, M. A. Ulrickson, and J. H. Bullock, Thermalhydraulic optimization of hypervapotron geometries for first wall applications, 24<sup>th</sup> IEEE/NPSS Symposium on Fusion Engineering, 2011, pp. 1-6.
- [4.] R. D. Boyd, Subcooled flow boiling critical heat flux (CHF) and its application to fusion energy components. Part I. A review of fundamentals of CHF and related data base, *Fusion Technology*, Vol. 7, 1985, pp. 7-30.
- [5.] R. D. Boyd, Subcooled flow boiling critical heat flux (CHF) and its application to fusion energy components. Part II. A review of microconvective, experimental, and correlational aspects, *Fusion Technology*, Vol. 7, 1985, pp. 31-52.
- [6.] J. Milnes, A. Burns, and D. Drikakis, Computational modeling of the hypervapotron cooling technique, Vol. 87, 2012, pp. 1647-1661.
- [7.] J. Milnes, D. Drikakis, Qualitative assessment of RANS models for hypervapotron flow and heat transfer, *Fusion Engineering and Design*, 84 (2009) 1305-1312.
- [8.] L. Tao, Y. Xie, C. Hu, et al., Numerical analysis of a cooling system for high heat flux components in the neutral beam injection system, *Fusion Engineering and Design*, Vol. 85, 2010, pp. 2095-2099.

- [9.] R. D. Boyd, Thermal management using a hypervapotron; Part I: some controlling parameters, Nuclear and Emerging Technologies for Space (NETS-2013), Paper 6903, 2013.
- [10.] D. L. Youchison, M. A. Ulrickson, and J. H. Bullock, A comparison of two-phase computational fluid dynamic codes applied to the ITER first wall hypervapotron, IEEE Transactions on Plasma Science, Vol. 38, Iss. 7, 2010, pp. 1704-1708.
- [11.] S. Pascal-Ribot, A. F. Saroli, M. Grandotto, et al., 3D numerical simulations of hypervapotron cooling concept, Fusion Engineering and Design, Vol. 82, 2007, pp. 1781-1785.
- [12.] I. B. Ovchinnikov, D. E. Bondarchuk, A. A. Gervash, et al., ITER FW cooling by a flat channel, adapted to low flow rate and high pressure drop, Fusion Engineering and Design, Vol. 86, 2011, pp. 2971-2982.
- [13.] D. W. Lee, Y. D. Bae, S. K. Kim, et al., Design evaluation of the semi-prototype for the ITER blanket first wall qualification, Journal of Thin Solid Films, Vol. 518, 2010, pp. 6676-6681.
- [14.] D. W. Lee, Y. D. Bae, S. K. Kim, et al., Experimental and analysis of hypervapotron mock-ups for preparing the 2nd qualification of the ITER blanket first wall, Fusion Engineering and Design, Vol. 85, 2010, pp. 2155-2159.
- [15.] Z. W. Wang, Y. T. Song, and S. H. Huang, Analysis and experiment of the hypervapotron mock-up for the EAST upgrade, 24<sup>th</sup> IEEE/NPSS Symposium on Fusion Engineering SP2-10, 2011, pp. 1-4.
- [16.] I. Mazul, A. Alekseev, V. Belyakov et al., Russian development of enhanced heat flux technologies for ITER first wall, Fusion Engineering and Design, (Article In Press).
- [17.] G. Cattadori, G. P. Gaspari, G. P. Celata et al., Hypervapotron technique in subcooled flow boiling CHF, Experimental Thermal and Fluid Science, Vol. 7, 1993, pp. 230-240.
- [18.] F. Escourbiac, I. B. Vastra, V. Kuzentsov, et al., A mature industrial solution for ITER divertor plasma facing components: Hypervapotron cooling concept adapted to Tore Supra flat tile technology, Fusion Engineering and Design, Vol. 75-79, 2005, pp. 387-390.
- [19.] F. P. Incropera, D. P. Dewitt, T. L. Bergman et al., Fundamentals of Heat and Mass Transfer, 6<sup>th</sup> Edition, John Wiley & Sons, 2007, pp. 144-154.
- [20.] F. Escourbiac, J. Schlosser, M. Merola, et al., Experimental optimisation of a hypervapotron concept for ITER plasma facing components, Fusion Engineering and Design, Vol. 66-68, 2003, pp. 301-304.
- [21.] A. Ulas, E. Boysan, Numerical analysis of regenerative cooling in liquid propellant rocket engines, Aerospace Science and Technology (In Press).

